

A Self-consistent Model in the Local Residual Stress Evaluation of 316H Stainless Steel

Jianan Hu^{1,*}, Bo Chen², David Smith², Peter Flewitt³, Alan C.F. Cocks¹

¹ Department of Engineering Science, University of Oxford, OX1 3PJ, UK

² Department of Mechanical Engineering, University of Bristol, BS8 1TR, UK

³ IAC, University of Bristol, BS8 1TR, UK

* Corresponding author: jianan.hu@eng.ox.ac.uk

Abstract The residual stresses in materials have a considerable effect on the mechanical properties, including creep and failure behaviour. Due to elastic and plastic anisotropy, differently oriented grains will exhibit different mechanical responses for a given macroscopic stress, leading to a variation of stresses within the grains. Experimental studies of meso-scale residual stress evolution can be used to validate crystal based plasticity and hardening models. In this paper, a self-consistent model and a simple multi-bar system are employed to determine how the evolution of the residual stress field depends on the constitutive assumptions for the individual grains. This framework has been used to evaluate data for the lattice strain evolution in 316H stainless steel measured from neutron diffraction experiments. A suitable model is identified, which captures the macroscopic response of the material and explains the way in which the meso-scale residual stresses evolve. The good agreement achieved between the self-consistent model and experiment demonstrates that this model reasonably reflects the mechanical physics of 316H stainless steel, and may help improve our understanding of the influence of the residual stress on the fracture and failure behaviour.

Keywords Residual stress, Self-consistent model, 316H stainless steel, Neutron diffraction

1. Introduction

Residual stresses developed within grains of a polycrystalline material have a considerable effect on material properties, including load carrying capacity, creep and crack initiation and propagation [1]. Thus, understanding the distribution and the evolution of residual stresses is vital to assessing the performance of engineering components. Elastic and plastic anisotropy of the differently oriented grains results in a variation in the mechanical response of different grains and the development of meso-scale intragranular residual stresses [2,3], i.e. the stresses within the grains. The development of these residual stresses depends on the detailed flow, hardening and recovery laws for the different slip systems in the body. A number of techniques have been developed for measuring residual stresses (or residual elastic strains) in a body. Neutron diffraction can provide information about the residual elastic strains in different families of grains within the bulk of a polycrystalline sample. Availability of the data offers the opportunity to identify the most appropriate forms of constitutive relationships for the individual grains, which can then be used to predict the evolution of residual stresses and the macroscopic material response under complex thermo-mechanical loading histories.

Various models have been proposed or developed to predict quantitative and qualitative features of the elastic-plastic behaviour of polycrystalline materials, such as Taylor model [4], which assumes that all grains experience identical strain, but elastic anisotropy plays no role. Self-consistent models which employ solutions of the classical Eshelby inclusion problem [5,6], have been employed extensively to describe the structure-property relationship of materials. Examples of this approach are given by Kroner [7], and Budiansky and Wu [8] to describe the effect of misfit strain on plastic deformation. However, the inclusion is simplified as being elastically isotropic and with the same properties as the matrix. Self-consistent models, suggested by Hill [9] and Hutchinson [10],

incorporate a more elaborate description of single crystal behaviour for calculating the stresses and strains in the individual grains, but with no physical description of work hardening. The physical characterization of work hardening is discussed by Kocks and Mecking [11], based on dislocation multiplication and the evolution of dislocation density. Lagneborg's dislocation link length model [12] provides a more detailed description of the dislocation structure and evolution of the structure based on Orowan bowing [13] and recovery of the dislocation structure.

In this paper, a self-consistent model is developed to consider both elastic and plastic anisotropy of the polycrystalline grains. A hardening model is described based on Lagneborg's dislocation link length model. A simplified multi-bar representation of the polycrystal is also described. Both these models are used to predict the elastic-plastic responses and the development of meso-scale residual stresses of a Type 316H stainless steel under uniaxial tensile loading. These models are validated using elastic lattice strain and residual lattice strain data obtained by the neutron diffraction technique. A detailed description and explanation of the experiment is presented in the companion paper [14]. The ability of these models to capture the observed response is discussed.

2. Formulation of the self-consistent model

In the self-consistent approach, each individual grain of a polycrystalline material, is regarded as a spherical inclusion in an infinite homogeneous matrix with the average macroscopic properties [7,8]. The purpose of the Eshelby based deformation model is to establish the relationship between the local individual grain-scale responses and the polycrystal aggregate response.

2.1. Model of elasticity

Eshelby obtained the solution for the elastic field of a misfitting (with a stress-free transformation strain ε^t) ellipsoidal homogeneous inclusion embedded in an infinite isotropic matrix of the same elastic constants. The total strain in the inclusion is linked by the transformation strain and a 6th-order tensor S^i relating the final constrained inclusion shape to the original shape mismatch between the matrix and the inclusion, and is only dependent on the geometry of the inclusion and Poisson's ratio of the medium [5,15]. For an inhomogeneity (a single inhomogeneous grain in the model) with different elastic constants containing a transformation strain ε^{ta} , its elastic field can be simulated by an equivalent homogeneous inclusion with a properly chosen transformation strain ε^{t*} . Given a macroscopically applied stress σ , the relationship between the real transformation strain in the inhomogeneity and the virtual transformation strain in the equivalent inclusion can be derived as

$$\varepsilon^{ta} + \left[(C^a)^{-1} - (C^i)^{-1} \right] T \sigma = \left[(C^a)^{-1} C^i (I - S^i) + S^i \right] \varepsilon^{t*} \quad (1)$$

where C^a, C^i are respectively the stiffness matrices of the grain and the surrounding matrix. T is the orientation matrix of the grain described by the three Euler angles. I is the unity matrix. If the deformation is fully elastic, i.e. $\varepsilon^{ta} = 0$, ε^{t*} can be solved and the relationship between the applied stress and the grain stress and strain can be established

$$\sigma^a = \left\{ \left[\left[I - (S^i)^{-1} \right]^{-1} (C^i)^{-1} - (C^a)^{-1} \right]^{-1} \left[(C^a)^{-1} - (C^i)^{-1} \right] + I \right\} T \sigma = H^a T \sigma \quad (2)$$

$$\varepsilon^a = \left\{ (C^i)^{-1} + \left[\left[(C^a)^{-1} - (C^i)^{-1} \right]^{-1} (C^a)^{-1} C^i (S^i)^{-1} - C^i \right]^{-1} \right\} T \sigma = K^a T \sigma \quad (3)$$

where $H^a = \left\{ \left[\left[I - (S^i)^{-1} \right]^{-1} (C^i)^{-1} - (C^a)^{-1} \right]^{-1} \left[(C^a)^{-1} - (C^i)^{-1} \right] + I \right\}$ and

$$K^a = (C^i)^{-1} + \left\{ \left[(C^a)^{-1} - (C^i)^{-1} \right]^{-1} (C^a)^{-1} C^i (S^i)^{-1} - C^i \right\}^{-1}$$

2.2. Model of plasticity

The expression of the transformation strain in the grain has been considered to be the plastic misfit strain between the grain and the matrix in the same coordinate [7,8]

$$\varepsilon^{ta} = \varepsilon^p - T^{-T} E^p \quad (4)$$

where ε^p is the local plastic strain in the grain and E^p is the polycrystal plastic strain obtained by the volume average over all the grains with possible orientations. In Eq. (1), if $\varepsilon^{ta} \neq 0$, i.e. the material is plastically deformed, a relationship between ε^{t*} and the real plastic misfit strain ε^{ta} can be obtained by macroscopically unloading the sample (i.e. setting $\sigma = 0$). Further, the residual stress in the grain (X^a) can be derived as a function of the plastic misfit strain ε^{ta}

$$X^a = C^i (I - S^i) \left((C^a)^{-1} C^i S^i - (C^a)^{-1} C^i - S^i \right)^{-1} \varepsilon^{ta} \quad (5)$$

2.3. Crystal based plasticity model

Plastic deformation is the glide of dislocations on multiple slip systems [11,16]. Following the classical crystal plasticity model [16,17], the shear strain rate ($\dot{\gamma}^\beta$) of a slip system β ($\beta = 1 \sim m$, m : total number of slip systems) is related to the resolved shear stress (RSS, τ^β) and the critical resolved shear stress (CRSS, τ_{crss}^β) of the corresponding slip system by the power-law relationship

$$\dot{\gamma}^\beta = \dot{\gamma}_0 \left| \frac{\tau^\beta}{\tau_{crss}^\beta} \right|^t \text{sgn}(\tau^\beta) \quad (6)$$

where $\dot{\gamma}_0$ is a reference shear strain rate and t is the rate sensitivity exponent. As $t \rightarrow \infty$ this constitutive response of each slip system is consistent with rate-independent deformation [17]. In the computations here a value of $t=600$ is used to provide a response that is essentially rate independent for the timescales employed in the simulations. If $\bar{n}^\beta (n_1^\beta, n_2^\beta, n_3^\beta)$ is the normal direction and $\bar{s}^\beta (s_1^\beta, s_2^\beta, s_3^\beta)$ is one of the slip directions associated with the slip system β , the shear strain rate $\dot{\gamma}^\beta$ on this slip system provides a contribution to the plastic strain rate given by:

$$\dot{\varepsilon}^\beta = \text{sym}(\dot{\gamma}^\beta \bar{n}^\beta \otimes \bar{s}^\beta) = \theta^\beta \dot{\gamma}^\beta \quad (7)$$

where θ^β is the Schmid factor of the slip system, which also links the RSS with the stress of each individual grain [16,17]. The total plastic strain rate is the sum of $\dot{\varepsilon}^\beta$ over all the slip systems

$$\dot{\varepsilon}^p = \sum_{\beta} \dot{\varepsilon}^\beta = \sum_{\beta} \theta^\beta \dot{\gamma}^\beta \quad (8)$$

The controlling parameters for slip are the CRSS and the hardening law. The initial CRSS is assumed to be the same on all slip systems and it is taken to evolve as [9]

$$\dot{\tau}_{crss}^i = \sum_j h^{ij} |\dot{\gamma}^j| \quad \text{with} \quad h^{ij} = h(q + (1-q)\delta^{ij}) \quad (9)$$

where h^{ij} is the rate of strain hardening on slip system i due to a shearing on slip system j [16]. The summation is over all active slip systems. h is the hardening coefficient dependent on the previous deformation history and q is a factor determining the degree of latent hardening: $q=0$ provides only self-hardening, $q=1$ represents Taylor hardening, and $q>1$ gives stronger latent hardening. For latent hardening, the range of q has been reported to be $1 < q < 1.4$ [17,18]. As for the coefficient h , the specific form needs to be given by the physical hardening model.

2.4. Dislocation link length based hardening model

The strain hardening effect is physically characterized by the motion of mobile dislocations. The dislocation link length model originally proposed by Lagneborg [12] offers a reasonable illustration of such an effect. A dislocation link is defined as the segment between two pinning points (dislocation junctions or other obstacles). The hardening behaviour is characterized by the evolution of the distribution of dislocation link lengths associated with a particular slip system.

2.4.1. The structure of dislocation link distribution

In the model, the dislocation structure can be described as a population of dislocation links with spacing occurring as a spectrum of lengths, i.e. a 3D dislocation network [12]. The distribution of link lengths in the network is described by an instantaneous distribution function $\phi(\lambda)$, defined such that $\phi(\lambda)d\lambda$ equals the number of links per unit volume with lengths between λ and $\lambda + d\lambda$. The detailed form of the distribution function can be expressed as [19,20]

$$\phi(\lambda) = A\lambda^2 e^{-B\lambda^2} \quad (10)$$

where A and B are two constants which evolve during deformation. A typical distribution is shown in Fig. 1(a), as a truncated Weibull distribution. λ_{th} is the threshold or the current maximum link length on a slip system, directly related to the current CRSS on the corresponding system.

$$\lambda_{th} = \frac{\alpha Gb}{\tau_{crss}} \quad (11)$$

where α is a dimensionless constant determining the strength of an obstacle, G is the shear modulus and b is the value of Burgers vector. The truncation in Fig. 1(a) indicates that no links longer than the threshold links can exist in the complex network without recovery. Thus the total number (N) per unit volume and the total density (ρ) of dislocation links can be expressed as

$$N = \int_0^{\lambda_{th}} \phi(\lambda) d\lambda \quad \text{and} \quad \rho = \int_0^{\lambda_{th}} \lambda \phi(\lambda) d\lambda = N\bar{\lambda} \quad (12)$$

where $\bar{\lambda}$ is the average link length, or mean free path of dislocation motion [12,21,22]. Meanwhile, a constant volume boundary condition is required and expressed as [12,21]

$$\int_0^{\lambda_{th}} c\lambda^3 \phi(\lambda) d\lambda = 1 \quad (13)$$

where c is a geometric constant close to 1.

2.4.2. The dislocation unzipping movement

In Lagneborg's model, dislocation motion is described as long waiting times at the obstacles and occasional spurtlike movements of dislocation links between obstacles [12]. Thus at any instant, all the dislocations in the network can be considered as immobile and held up at obstacles. At a certain stress, dislocation links with the threshold length will be released and become mobile. They overcome the obstacles and then continue to glide and sweep out an area before being blocked and partitioned into shorter links by adjacent obstacles in the network, which become immobile again (Fig. 1b). If the area swept out by each released dislocation link is s , the shear strain rate is [12,22]

$$\dot{\gamma} = bs\dot{N}_m \quad (14)$$

where \dot{N}_m is the release rate of mobile links, which is related to the current value of CRSS and its rate of increase. The expression of s is complicated and not reproduced here. The Orowan bowing [13] process was assumed in Lagneborg's original model, where the released links expand to circular loops and the area is assumed to be $4\pi\bar{\lambda}^2$. However, such encircling movement is often the characterization for strong obstacles (large α) and the spatial distribution of obstacles is always a

random array for a wide range of strengths [23]. A consecutive release process (Fig. 1c) is observed for weak obstacles (such as forest dislocations), which is commonly referred to as an unzipping mechanism [23]. Although it describes a release process by links with various lengths besides the threshold one, it is assumed that this does not influence the activation criterion of the release process in the model, but only offers a greater sweeping area than the original Orowan bowing process. The sweeping area in the model is assumed to be a circular arch and the averaged distance a link can reach is proportional to $\bar{\lambda}$ but needs to be determined by fitting with experimental data.

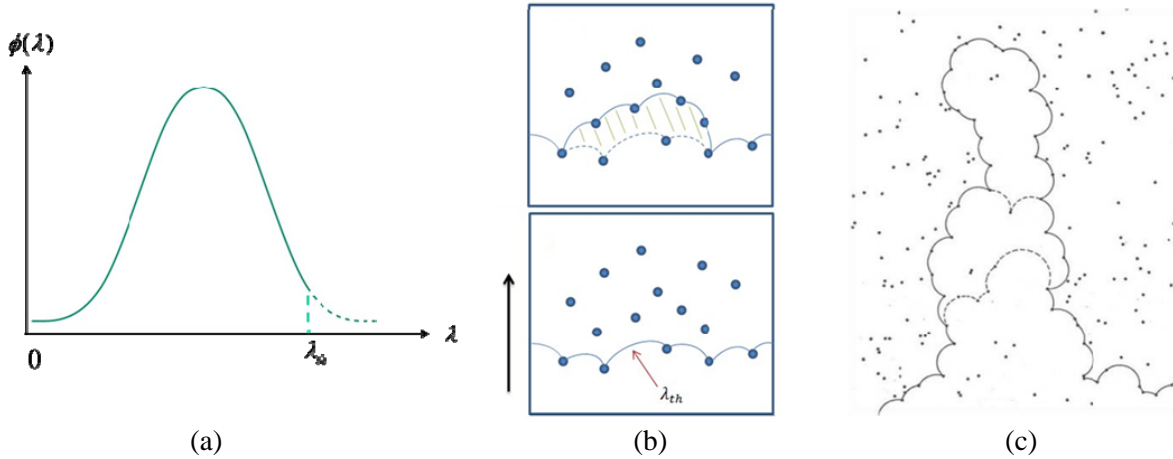


Figure 1. (a) Truncated Weibull dislocation distribution; (b) A schematic diagram of the kinetic motion of dislocation links before and after release, where the solid points are obstacles, e.g. dislocation junctions on other slip planes; (c) Unzipping movement of a dislocation which glides on a slip plane [23]

The evolution of the dislocation distribution function updates two state variables in the model: (1) the local threshold link length; (2) the global dislocation density. The dislocation multiplication is described by the generation and disappearance of links, which can be separated into different stages such as release, expansion and cut. The detailed model derivation for the structure evolution is not shown here. Finally, the relationship between the shear strain rate and the CRSS rate of increase on a single slip system can be derived from Eq. (14) as

$$\dot{\gamma} = f(\tau_{crss}, \rho, \dot{\rho}) \dot{\tau}_{crss} \quad (15)$$

Compared with Eq. (9), $1/f(\tau_{crss}, \rho, \dot{\rho}) = h$ is the hardening coefficient. In the simulation, a simple linear hardening is considered, which is given by an assumption that the total unzipped link length in a slip system and the link length at which the distribution function has the maximum value are proportional to the threshold link length. The model gives a range of linear hardening coefficients obtained by the variation of different parameters such as the obstacle strength α . However, the coefficient as a whole is treated as a fitting parameter in the simulation, but its value must lie within a physical range for this model to hold.

3. A simplified multi-bar system

A simplified and straightforward 1D multi-bar system which captures the general structure of the self-consistent model was established. The general structure the system is shown in Fig. 2. Taking an face centred cubic (fcc) material as an example, all the thick bars (with the properties of single cubic grains with their specific orientation and with equal cross-sectional area) are representative components of the isotropic polycrystal and their average response gives the polycrystal behaviour. The small bar in the system represents a grain family, which does not influence the averaged behaviour of the system since its cross-sectional area is negligible. Therefore, this system demonstrates the framework of the basic structure of a self-consistent model, a single grain

embedded in an infinite matrix with the averaged isotropic property, despite the difference that the geometric feature requires equal strain for all the bars which is similar to a Taylor model.

The elastic anisotropy for the multi-bar system is determined such that each bar has a different Young's modulus along the loading direction related to the individual orientation. Whilst for the plastic anisotropy, the classic 1D incremental plasticity model of isotropic hardening [24] is used, where the strain hardening effect is characterised by a plastic modulus defined as the instantaneous slope of the stress-strain curve after micro-yielding. For the multi-bar system, the assumption of linear hardening of each grain is described by an orientation-dependent bilinear response [24] and the plastic modulus serves as the hardening coefficient of this system.

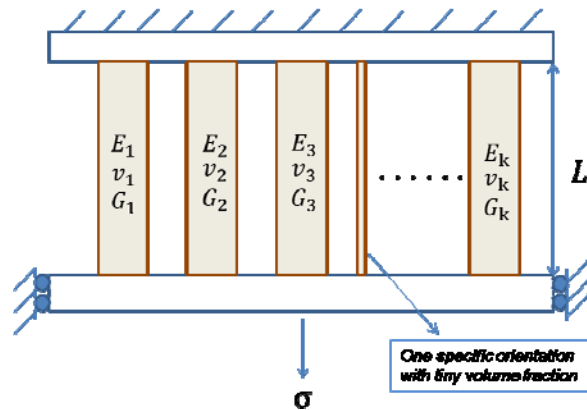


Figure 2. A schematic diagram of the multi-bar system

4. Model evaluation

4.1. Neutron diffraction experiment

To validate the self-consistent model, the lattice strain evolution, especially the residual lattice strain in different crystallographic planes of a fcc material of ex-serviced 316H stainless steel was measured using neutron diffraction (ND) combined with in-situ tensile deformation on the ENGIN-X instrument at the ISIS pulsed neutron facility, Rutherford Appleton Laboratory. A schematic diagram of the experimental setup is shown in Fig. 3.

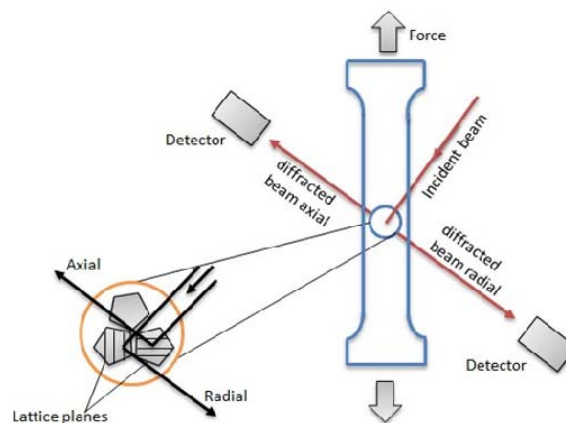


Figure 3. Schematic diagram of neutron diffraction experiment

The incident beam directed at a specimen consists of a polychromatic spectra with a continuous range of wavelengths, which enables the recording of many lattice planes in each measurement. The loading direction is horizontal and at 45° to the incident beam. Two detectors are positioned to

allow simultaneous measurement of lattice spacing both parallel (axial) and perpendicular (radial) to the loading direction. The lattice strain measured for each plane represents the average value of the elastic strain within a family of grains which are oriented such that a specific $\{hkl\}$ plane diffracts to the detector. For example, in the axial direction, a specific $\{hkl\}$ lattice strain indicates the average axial elastic strain over the grains located in the gauge volume with their $\{hkl\}$ plane normal parallel to the loading axis. The complete description of the experiment and the full range of measurement are presented in Ref [14].

4.2. Simulation of the experimental results

4.2.1. Macroscopic behaviour and parameter identification

In the present calculations, no lattice rotation or texture development was incorporated due to the small plastic deformation [25]. The property of the matrix was initially undetermined and was solved by iteration from the average response of all the grains. This then served as the standard for the selection of the number of bars in the multi-bar system. The latent hardening factor q was pre-set as 1, i.e. the hardening on all slip systems were equal, which is reasonable in the current framework since the expansion and partition of dislocation links may generate equal obstacles for all slip planes. The effect of different values of q was considered elsewhere [26]. The fitting process was to initially make the macroscopic stress-strain response of the self-consistent model resemble the actual measured macroscopic behaviour of the sample and then to use the refined parameters to predict the macroscopic behaviour of the multi-bar model and the microscopic behaviours of the local grain family in both models. The fitting parameters are listed in Table 1 together with the single crystal elastic constants of the fcc material 316H stainless steel. The calculated macroscopic stress-strain responses are shown in Fig. 4, with the results obtained by both the self-consistent and multi-bar models.

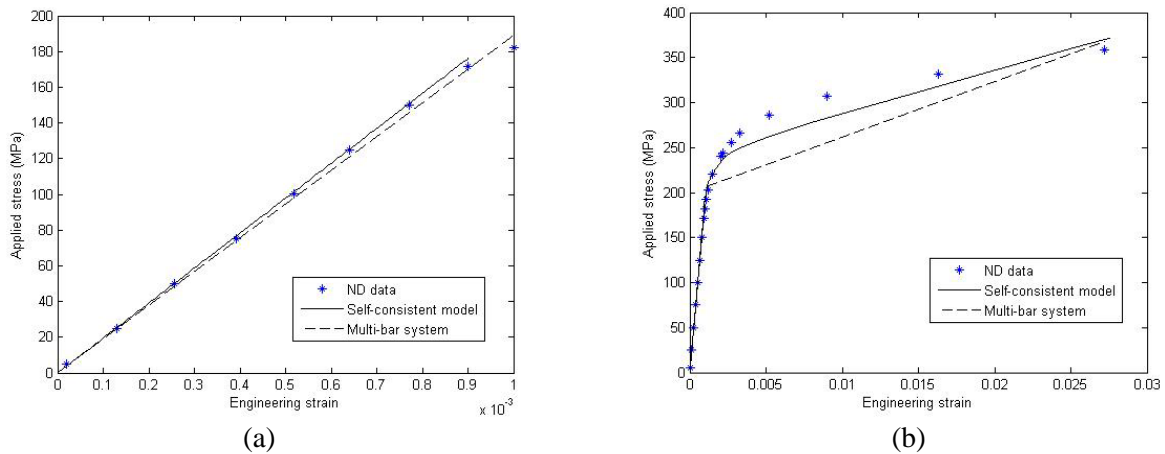


Figure 4. Macroscopic polycrystal stress-strain response of 316H stainless steel under uniaxial tension at room temperature; (a) the elastic region; (b) the whole region. (ND=neutron diffraction)

Table 1. Material parameters of 316H stainless steel used in the simulation

| C_{11} (GPa) | C_{12} (GPa) | C_{44} (GPa) | $\dot{\gamma}_0$ | t | τ_{crss0} (GPa) | b (m) | q | h (MPa) |
|----------------|----------------|----------------|------------------|-----|----------------------|---------|-----|-----------|
| 198 | 125 | 122 | 5e-6 | 600 | 82 | 2.5e-10 | 1 | 370 |

4.2.2. The grain family and the Young's modulus

The family of grains contributing to the reflection of a certain crystallographic plane in neutron diffraction has one uniform orientation along the measurement direction. The averaged response of

this grain family can be determined either by averaging the responses of all the members or by considering the family as a whole with an averaged transversely isotropic property. In the present simulation, the results of two representative grain families {220} and {111} with the aggregate normal along the axial direction were considered. The diffraction elastic constants were measured in the experiment, in which the Young's modulus was defined as the slope of the applied stress over the elastic lattice strain [2,3]. The experimental measurement and the model prediction results for the two grain families are listed in Table 2, where the theoretical value and model prediction of the physical Young's modulus is also presented as a further validation of the model.

Table 2 Measurement and prediction of the Young's modulus of {220} and {111} grain family

| Grain family | {220} | {111} |
|-------------------------------------|------------|------------|
| Diffraction Young's modulus (GPa) | 209.1±15.8 | 225.3±11.9 |
| Self-consistent model prediction | 210.8 | 241.8 |
| Physical Young's modulus (GPa) [27] | 196 | 285 |
| Self-consistent model prediction | 225.1 | 285.1 |

4.2.3. The residual lattice strain

The results of axial elastic lattice strain evolution during loading, together with the predictions of the self-consistent (blue solid line) and multi-bar (blue dash line) models are demonstrated in Fig. 5. At each unloading step, the residual axial elastic lattice strain for the grain families was measured and was then plotted against the macroscopic residual plastic strain (shown in Fig. 6 with the model prediction). Good agreement is observed between the experimental data and the prediction of self-consistent model, while the quality of the prediction of multi-bar model is a mixture.

From the figures, although multi-bar model gives a poorer prediction than the self-consistent model, both of the models capture the major trend of the experimental data, particularly the transition that occurs in both the lattice strain and the residual lattice strain evolution upon micro-yielding. In addition, the two models predict that both grain families have an initially increasing residual lattice strain evolution, which is when the surrounding matrix yields (or some grains in the matrix yield) before each grain family. The subsequently decreasing residual lattice strain is when all the grains deform plastically, which is reflected in the difference in the plastic misfit strains in Eq. (4).

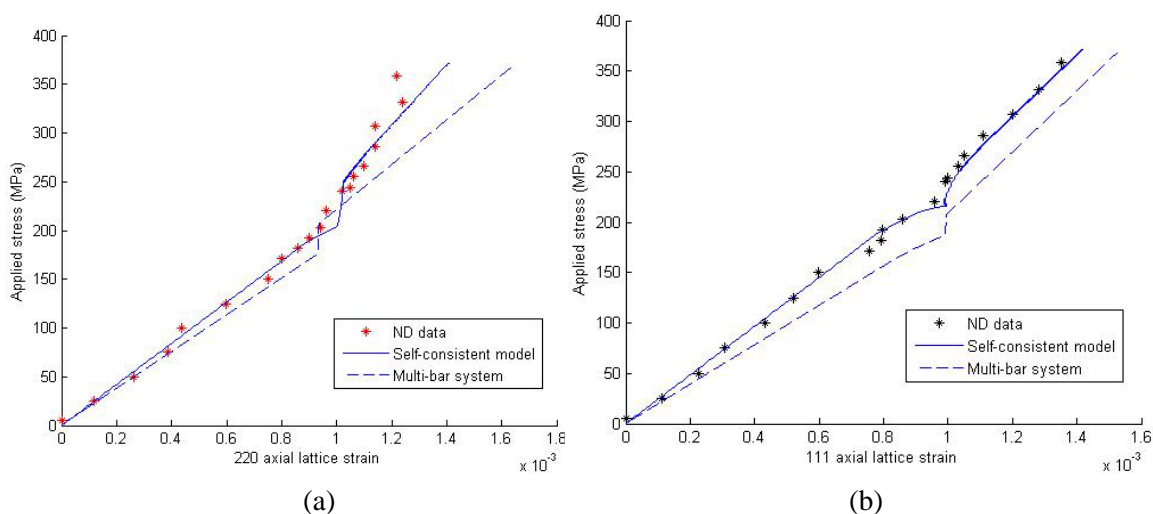


Figure 5. Neutron diffraction (ND) measurement and model prediction results of the applied stress vs axial lattice strain upon loading (a) {220} grain family; (b) {111} grain family.

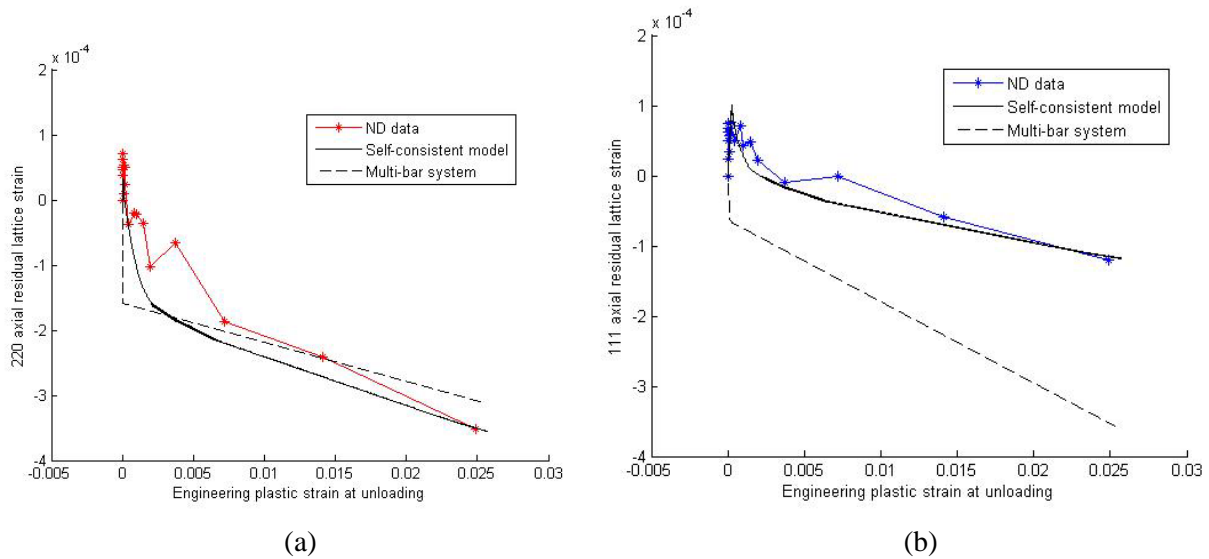


Figure 6. Neutron diffraction (ND) measurement and model prediction results of the axial residual lattice strain vs the engineering plastic strain at unloading. (a) {220} grain family; (b) {111} grain family.

5. Discussion and conclusion

The mechanical features of {220} and {111} grain families have been discussed in [2,3]. From the results, the linear hardening assumption is acceptable and permits only one parameter, the hardening coefficient h to be used. The oscillation of the residual elastic lattice strain at relatively small plastic strain region in the measurement is expected to be a result of a combination of experimental error and the complex interaction between grains. Since the self-consistent model only considers the interaction between one single grain and the whole matrix, such oscillations cannot be predicted by the model. The poorer predictions from the multi-bar system in Fig. 5-6 may result from the identical strain for all the bars, regardless of their stiffness and hardening responses. Despite the same applied stress and yield stress with those in the self-consistent model, the multi-bar system may display a different mechanical response, especially the accumulation of residual elastic lattice strain. Such a discrepancy demonstrates that the identical strain assumption may not be acceptable for the local residual lattice strain evaluation.

A self-consistent model for polycrystal deformation is established with specific emphasis on the elastic and plastic anisotropy. The self-consistent scheme includes the elastic-plastic interaction between the grains which are regarded as spherical inclusions in an infinite homogeneous matrix with the averaged polycrystal response. A simplified multi-bar system is introduced which captures the basic structure of the self-consistent model. The models predictions were compared with the neutron diffraction measurements of elastic lattice strains in grain families within an ex-serviced 316H stainless steel polycrystal subjected to uniaxial tensile loading. The good agreement between the measured and calculated lattice strains validates the self-consistent model.

Acknowledgements

ISIS is acknowledged for the provision of beamtime at Beamline ENGIN-X. The authors also wish to acknowledge the financial support from EDF Energy.

References

- [1] O. Kwon, B. Pathiraj, K.M. Nikbin, Effect of residual stress in creep crack growth analysis of cold bent tubes under internal pressure, *Int J Pres Ves Pip*, 78(2001) 343-350.
- [2] B. Clausen, T. Lorentzen, T. Leffers, Self-consistent modelling of the plastic deformation of f.c.c

- . polycrystals and its implications for diffraction measurements of internal stresses, *Acta Mater*, 22 (1998) 3087-3098.
- [3] M.R. Daymond, P.J. Bouchard, Elastoplastic deformation of 316 stainless steel under tensile loading at elevated temperatures, *Metall Mater Trans A*, 37 (2006) 1863–1873.
- [4] G.I. Taylor, Plastic strain in metals, *J Inst Metals*, 62(1938) 307-325.
- [5] J.D. Eshelby, The determination of the Elastic Field of an Ellipsoidal Inclusion and Related Problems. *Proc R Soc Lond A*, 241 (1957) 376–396.
- [6] P.J. Withers, W.M. Stobbs, O.B. Pedersen, The application of the Eshelby method of internal stress determination to short fibre metal matrix composites, *Acta Metall*, 37(1989) 3061-3084.
- [7] E. Kroner, On the plastic deformation of polycrystals, *Acta Metall*, 9(1961) 155-161.
- [8] B. Budiansky, T.T. Wu, Theoretical prediction of plastic strains of polycrystals, *Proc. 4th Congr Appl Mech*, 1962 1175-1185.
- [9] R. Hill, Generalized constitutive relations for incremental deformation of metal crystals by multislip, *J Mech Phys Solids*, 14(1966) 95-102.
- [10] J.W. Hutchinson, Elastic-plastic behaviour of polycrystalline metals and composites, *Proc Roy Soc Lond A*, 319 (1970) 247-272.
- [11] U.F. Kocks, H. Mecking, Physics and phenomenology of strain hardening: the FCC case, *Progress in Materials Science*, 48(2003) 171-273
- [12] R. Lagneborg, B.H. Forsen, A model based on dislocation distributions for work-hardening and the density of mobile and immobile dislocations during plastic flow, *Acta Metall*, 21(1973) 781-790.
- [13] E. Orowan, The creep of metals, *J West Scotland Iron Steel Inst*, 54(1946-1947) 45-96.
- [14] B. Chen, D.J. Smith, P.E.J. Flewitt, S.Y. Zhang, Measurement of internal stress and internal resistance resulting from creep of Type 316H stainless steel, 13th Int. Conf. Fract., Beijing, (2013).
- [15] T. Mura, *Micromechanics of Defects in Solids*, Martinus Nijhoff Publishers, 1982.
- [16] R.J. Asaro, A. Needleman, Texture development and strain hardening in rate dependent polycrystals, *Acta Metall*, 33(1985) 923-953.
- [17] J.W. Hutchinson, Bounds and self-consistent estimates for creep of polycrystalline materials, *Proc R Soc Lond. A* 348(1976) 101-127.
- [18] C.A. Bronkhorst, S.R. Kalidindi, L. Anand, Polycrystalline plasticity and the evolution of crystallographic texture in fcc metals, *Phil Trans R Soc Lond A*, 341(1992) 443-477.
- [19] L. Shi, D.O. Northwood, On dislocation link length statistics for plastic deformation of crystals, *Phys Stat Sol A*, 137(1993) 75-85.
- [20] B.S. Wang, F.Y. Sun, Q.E. Meng, W.C. Xu, An approach to theoretical function of dislocation link length distribution in metal, *Acta Metall A*, 5(1992) 314-317.
- [21] A.J. Ardell, M.A. Przystupa, Dislocation link length statistics and elevated temperature deformation of crystals, *Mech Mater*, 3(1984) 319-332.
- [22] O. Ajaja, A dislocation network model of recovery-controlled creep, *J Mater Sci*, 21(1986) 3351-3356.
- [23] A.J.E. Foreman, M.J. Makin, Dislocation movement through random arrays of obstacles, *Philos Mag*, 14 (1966) 911-924.
- [24] J.C. Simo, T.J.R. Hughes, *Computational inelasticity*, Springer-Verlag, New York, 1998.
- [25] B. Clausen, Characterization of polycrystal deformation, PhD thesis, Riso National Laboratory, Roskilde, Denmark, 1997.
- [26] D.F. Li, N.P.O. Dowd, On the evolution of lattice deformation in austenitic stainless steels—The role of work hardening at finite strains, *J Mech Phys Solids*, 59(2011) 2421-2441.
- [27] G.E. Dieter, *Mechanical Metallurgy*, McGraw-Hill Book Co., New York, 1986.